Activity-dependent inhibitory synapse remodeling through gephyrin phosphorylation

Carmen E. Flores[a], Irina Nikonenko[a], Pablo Mendez[a], Jean-Marc Fritschy[b], Shiva K. Tyagarajan[b,1], and Dominique Muller[a,1,2]

[a]Département des Neurosciences Fondamentales, Faculté de Médecine, Centre Médical Universitaire, Université de Genève, 1211 Geneve 4, Switzerland; and [b]Institute of Pharmacology and Toxicology, University of Zürich, 8057 Zurich, Switzerland

Edited by Richard L. Huganir, The Johns Hopkins University School of Medicine, Baltimore, MD, and approved December 2, 2014 (received for review June 20, 2014)

Maintaining a proper balance between excitation and inhibition is essential for the functioning of neuronal networks. However, little is known about the mechanisms through which excitatory activity can affect inhibitory synapse plasticity. Here we used tagged gephyrin, one of the main scaffolding proteins of the postsynaptic density at GABAergic synapses, to monitor the activity-dependent adaptation of perisomatic inhibitory synapses over prolonged periods of time in hippocampal slice cultures. We find that learning-related activity patterns known to induce N-methyl-d-aspartate (NMDA) receptor-dependent long-term potentiation and transient optogenetic activation of single neurons induce within hours a robust increase in the formation and size of gephyrin-tagged clusters at inhibitory synapses identified by correlated confocal electron microscopy. This inhibitory morphological plasticity was associated with an increase in spontaneous inhibitory activity but did not require activation of $GABA_A$ receptors. Importantly, this activity-dependent inhibitory plasticity was prevented by pharmacological blockade of Ca^{2+}/calmodulin-dependent protein kinase II (CaMKII), it was associated with an increased phosphorylation of gephyrin on a site targeted by CaMKII, and could be prevented or mimicked by gephyrin phosphomutants for this site. These results reveal a homeostatic mechanism through which activity regulates the dynamics and function of perisomatic inhibitory synapses, and they identify a CaMKII-dependent phosphorylation site on gephyrin as critically important for this process.

inhibition | gabaergic synapse | plasticity | hippocampus | CaMKII

Several activity-dependent plasticity and homeostatic mechanisms (1, 2) contribute to regulate synaptic strength at excitatory synapses. Similar mechanisms are also expected to finely tune the level of inhibition in response to activity in individual neurons, but the mechanisms remain poorly understood. Different forms of plasticity at GABAergic synapses have been reported based on either presynaptic or postsynaptic mechanisms (3, 4). Similar to receptors at excitatory synapses, $GABA_A$ receptors ($GABA_A$Rs), which mediate the fast component of inhibitory transmission, display complex trafficking mechanisms that affect the surface localization and diffusion of receptors (5). The distribution and clustering of $GABA_A$Rs at synapses is tightly regulated through interactions with the scaffolding protein gephyrin, one of the main structural constituent of inhibitory postsynaptic densities. Gephyrin forms multimeric complexes that allow the anchoring of $GABA_A$Rs (6) via molecular mechanisms that include phosphorylation and interactions with the guanine-nucleotide exchange factor collybistin (7–12). In addition to changes in inhibitory strength, more recent in vivo experiments revealed that inhibitory synapses are also dynamic structures that can be formed and eliminated in response to sensory experience (13–15). The mechanisms implicated in the coordinated regulation of excitatory and inhibitory plasticity remain, however, poorly understood. We investigated here this issue by using repetitive confocal imaging of tagged gephyrin to monitor the dynamic behavior of perisomatic inhibitory synapses over periods of days. Our results show that induction of synaptic plasticity and neuronal activity induces the formation of newly formed inhibitory synapses through postsynaptic mechanisms involving the phosphorylation of gephyrin at a CaMKII-dependent site.

Results

Turnover and Correlated Confocal Electron Microscopy of Gephyrin Clusters. We transfected rat hippocampal slice cultures with fluorescently tagged gephyrin, and 8 d after transfection, we monitored the behavior of identified gephyrin clusters over several days (Fig. 1 *A* and *B*). These analyses revealed that gephyrin clusters are dynamic structures that are continuously formed and eliminated over time. The basal level of turnover observed in 19 d in vitro (DIV19) slices averaged 13.6 ± 3.5% for newly formed clusters and 18.1 ± 3.8% for eliminated clusters (Fig. 1*C* and Table S1) per 24 h. This turnover occurred without significant changes in either cluster density or size over time (Fig. 1 *D* and *E*). As illustrated in Fig. 1*A*, gephyrin clusters showed large variations in size. The vast majority of clusters (>90%) were of small size (<0.5 μm^2), corresponding to the size of gephyrin clusters revealed by immunofluorescence (Fig. S1) or by quantitative nanoscopic imaging (16). To verify that fluorescent gephyrin clusters corresponded to inhibitory synapses, we used a correlated confocal electron microscopy (EM) approach to reconstruct dendritic segments of transfected pyramidal neurons (Fig. 1*F*). Inhibitory synapses were identified by the presence of a symmetric apposition between a postsynaptic density and a presynaptic terminal, filled with pleomorphic synaptic vesicles forming an active zone (17). A high level of correlation was observed between the presence of gephyrin clusters and the

Significance

Learning mechanisms rely on plasticity properties of excitatory synapses and an activity-dependent rewiring of excitatory networks. Inhibitory synapses also display plasticity properties, but it remains unknown whether and how excitatory activity and plasticity can affect the organization of inhibitory networks. Here we show that synaptic and neuronal activity directly regulates the number and function of perisomatic inhibitory synapses through a mechanism that involves the phosphorylation of gephyrin by the enzyme calcium/calmodulin-dependent protein kinase II. The results identify a homeostatic mechanism through which cell activity can continuously adjust its excitation/inhibition balance.

Author contributions: C.E.F., J.-M.F., S.K.T., and D.M. designed research; C.E.F., I.N., P.M., S.K.T., and D.M. performed research; J.-M.F. and S.K.T. contributed new reagents/analytic tools; C.E.F., I.N., P.M., S.K.T., and D.M. analyzed data; and C.E.F., S.K.T. and D.M. wrote the paper.

The authors declare no conflict of interest.

This article is a PNAS Direct Submission.

[1]S.K.T. and D.M. contributed equally to this work.

[2]To whom correspondence should be addressed. Email: dominique.muller@unige.ch.

This article contains supporting information online at www.pnas.org/lookup/suppl/doi:10.1073/pnas.1411170112/-/DCSupplemental.

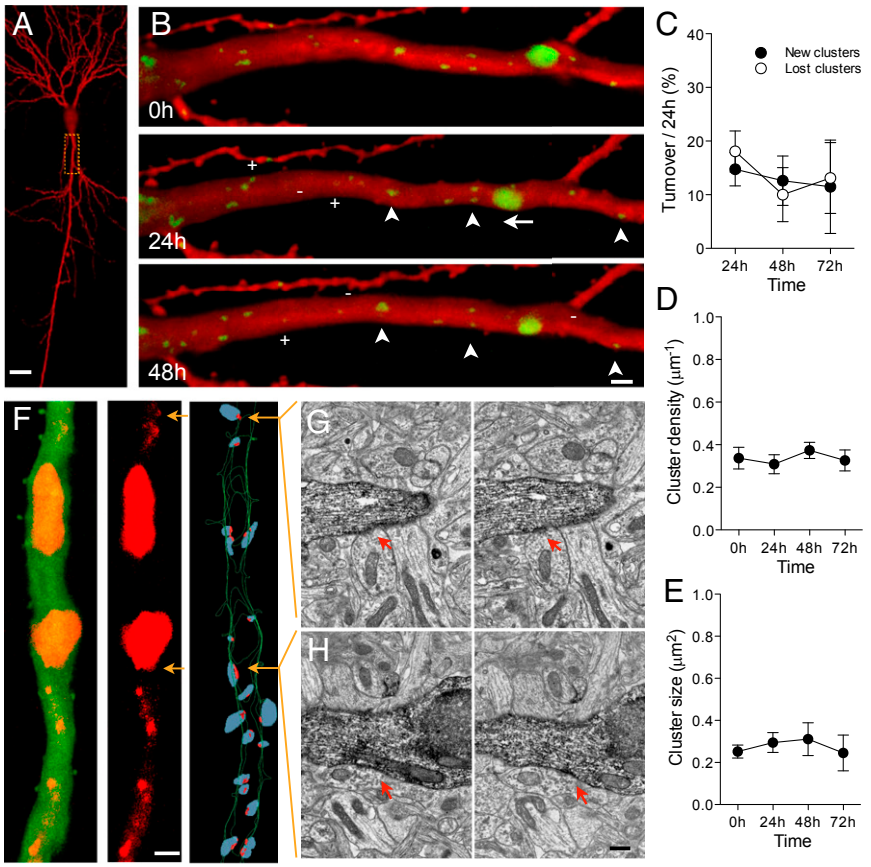

Fig. 1. Basal turnover of gephyrin-containing inhibitory synapses in rat organotypic hippocampal cultures. (*A*) Low maginification view of a mRFP-transfected CA1 pyramidal neuron imaged 8 d after transfection at 19 DIV. (*B*) Repetitive imaging at 24 h interval of the proximal dendrite of a eGFP-gephyrin transfected neuron. Note the variations in size of gephyrin clusters (green) and the existence of movements (arrow), stable (arrowheads), new (+), and lost (-) clusters. (*C*) Quantitative analysis of gephyrin turnover expressed as the fraction of new (filled circles) and lost (open circles) clusters observed over 24 h per proximal dendrite (n = 11 cells/134 clusters). (*D*) Absence of changes in cluster density under basal conditions. (*E*) Absence of changes in the mean size of gephyrin clusters. (*F Left*) Confocal projection of an apical proximal dendrite of a pyramidal neuron transfected with eGFP and mCherry-gephyrin. *Middle* shows only the mCherry-gephyrin signal, and *Right* illustrates the 3D EM reconstruction of the same dendrite. Red dots represent inhibitory symmetrical synapses and blue dots are the superimposed presynaptic boutons. Note that all small gephyrin clusters correlate with inhibitory synapses, whereas the large gephyrin clusters correspond to gephyrin accumulations in areas where multiple inhibitory synapses are present. (*G*) Electron microscopic image of the small confocal gephyrin cluster illustrated by the top arrow on *F Right*. The reconstructed dendrite was identified through eGFP immunolabeling. (*H*) Same but for the large inhibitory synapse corresponding to the large gephyrin cluster illustrated in *F* (lower arrow). (Scale bars: *A*, 10 µm; *B* and *F Left*, 2 µm; *H*, 0.2 µm.)

identification of inhibitory synapses. All gephyrin clusters, including very small ones (Fig. 1*G*) had at least one corresponding inhibitory synapse identified at the EM level. Large clusters (Fig. 1*H*; >1.5 µm^2) usually correlated with the presence of several inhibitory synapses and were excluded from quantitative analyses. Only few inhibitory synapses observed at the EM level had no detectable corresponding fluorescent signal (87.5% correlation between EM synapses and confocal clusters). This result confirmed to us that under our experimental conditions, gephyrin transfection did not affect its membrane trafficking and synapse localization (8).

Activity-Dependent Formation of New Gephyrin Clusters. We then investigated whether synaptic activation of transfected neurons could affect the dynamics of gephyrin clusters. We used two learning-related protocols previously shown to promote structural plasticity of excitatory synapses (18). A first protocol, carbachol treatment (Cch; 10 µM for 45 min) induced theta activity and produced a significant increase in the proportion of new gephyrin clusters detected over the next 24 h (Cch, n = 4 cells; Ctrl, n = 4 cells; Fig. 2 *A* and *C* and Table S1), but no significant changes in the proportion of lost clusters (Fig. 2*D* and Table S1). These turnover changes resulted in a significant increase in normalized density (1.8 ± 0.2 per 24 h) and were associated with an increase in size of gephyrin clusters (Fig. 2*E* and Table S1). Immunolabeling at 72 h for the presynaptic inhibitory marker GAD67 (glutamic acid decarboxylase) revealed a close apposition between all newly formed gephyrin clusters and GAD67 immunostaining (Fig. 2*F*), suggesting that they represented new inhibitory synapses.

A second protocol, induction of long-term potentiation by using theta burst stimulation (TBS; ref. 18), similarly produced a marked increase in the formation of new gephyrin clusters 24 h after stimulation (TBS, n = 7 cells; Fig. 2 *B* and *C* and Table S1), but no changes in the proportion of lost clusters (Fig. 2*D*). Additionally, preexisting gephyrin clusters showed a robust increase in size (Fig. 2*E* and Table S1). To verify that these new clusters represented inhibitory synapses, we performed 3D EM reconstruction of mCherry-gephyrin–transfected neurons following TBS. As illustrated in Fig. 3*G*, all new gephyrin clusters observed 24 h after TBS could be related to symmetric synapses or clusters of inhibitory contacts identified on 3D reconstruction, supporting the notion that they represented newly formed synapses. To determine the specificity of these changes, we also applied TBS, but in the presence of the *N*-methyl-D-aspartate (NMDA) receptor antagonist (D-AP5; 50 µM; Fig. S2). As shown

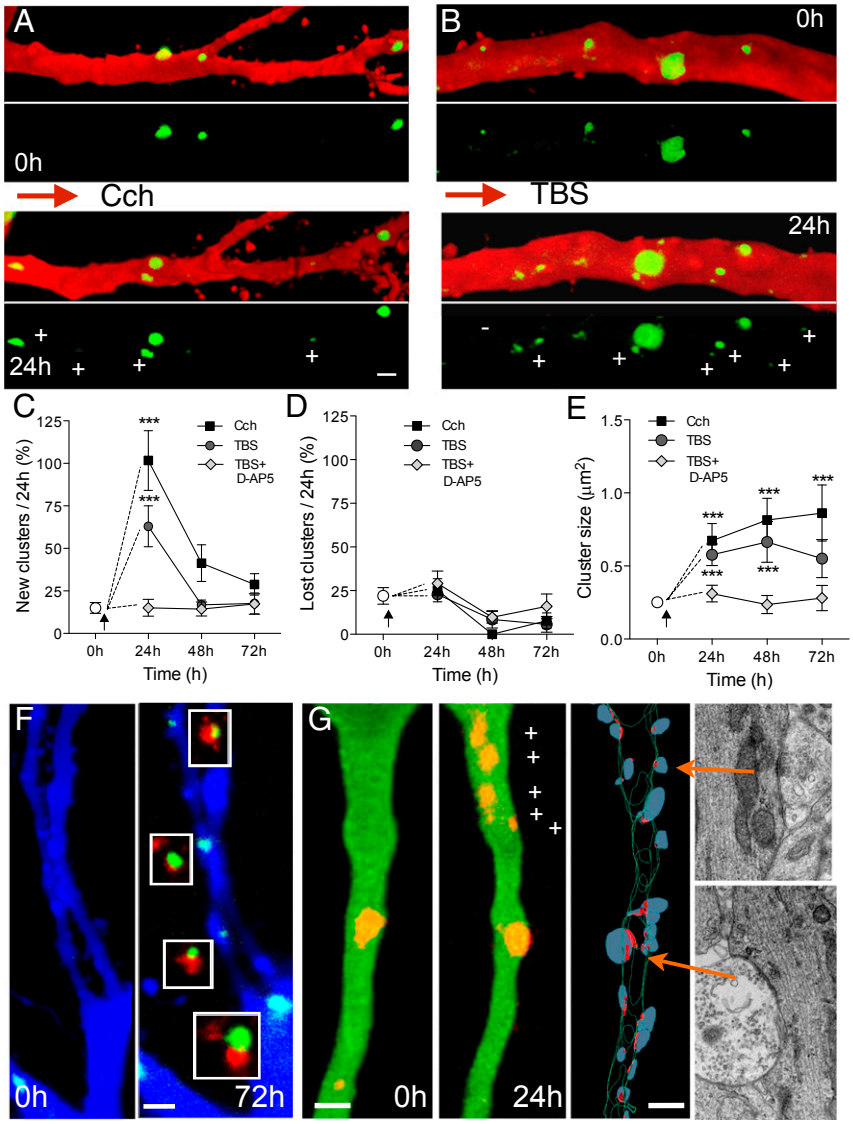

Fig. 2. Activity-dependent increase in gephyrin cluster dynamics. (*A*) Proximal apical dendrite illustrating the changes in eGFP-gephyrin clusters (+, new clusters; -, lost clusters) observed before and 24 h after application of 10 μM carbachol for 45 min. (*B*) Gephyrin cluster dynamics 24 h after TBS. (*C*) Proportion of newly formed gephyrin clusters observed per 24 h following Cch application (black squares), TBS (dark circles) and TBS in the presence of 50 μM D-AP5 (gray diamonds; one-way ANOVA with Bonferonni post hoc tests). (*D*) Changes in lost gephyrin clusters under the same conditions. (*E*) Changes in size of pre-existing gephyrin clusters (one-way ANOVA with Bonferonni post hoc tests). (*F*) Apposition of GAD67 immunostaining with the new gephyrin clusters induced by carbachol treatment (72 h after treatment). (*G*) New mCherry-gephyrin clusters (+) observed 24 h after TBS and correlated 3D-EM reconstruction of the same dendrite confirming the presence of inhibitory synapses. Red dots represent inhibitory symmetrical synapses, and blue dots represent presynaptic boutons. EM sections of two inhibitory synapses (arrows) are illustrated on the right. (Scale bars: 2 μm.)

in Fig. 3 *C*–*E*, D-AP5 prevented the increase in number (TBS, $n = 6$ cells) and size (Table S1) of gephyrin clusters.

Mechanisms Underlying Activity-Dependent Formation of New Gephyrin Clusters. To dissect the contribution of excitatory and inhibitory activity to this mechanism, we applied the $GABA_AR$ antagonist gabazine (GBZ), which enhances excitatory activity while blocking inhibition. Application of GBZ (15 μM, 45 min) to slice cultures also resulted in a robust increase in the formation of new gephyrin clusters over the next 24 h (GBZ, $n = 7$ cell, Fig. 3 *A* and *B* and Table S1) and an increase in their size (GBZ, Fig. 3*C* and Table S1). These changes could be detected within hours and were significant already 8 h after treatment (Fig. S3). To investigate the functional implications of this morphological inhibitory plasticity, we performed whole-cell recordings in GBZ-treated, nontransfected neurons. Analysis of spontaneous activity showed a significant increase in frequency (Ctrl, 1.06 ± 0.12 Hz, $n = 11$ cells; GBZ, 1.60 ± 0.19 Hz, $n = 11$ cells; $P < 0.05$; Fig. 3 *D* and *E*) and amplitude (Ctrl, 18.8 ± 1.9 pA, $n = 10$ cells; GBZ, 27.8 ± 2.9 pA, $n = 11$ cells; $P < 0.05$; Fig. 3 *D* and *E*) of miniature inhibitory postsynaptic currents (mIPSC), indicating that these new synapses were functional. Thus, postsynaptic activation of inhibitory synapses is not required for the induction of this inhibitory plasticity.

We then targeted individual pyramidal neurons and tested whether cellular activity, independently of synaptic inputs, could affect the dynamics of gephyrin-containing inhibitory synapses. Hippocampal cultures were cotransfected with mCherry-gephyrin and Channelrodhopsin-2 Venus (ChR2 Venus; Fig. 4*A*) and stimulated by using a 470-nm light pulse protocol (trains of five pulses at 10 Hz, repeated at 1 Hz for 5 min). This light stimulation paradigm reproducibly evoked action potentials in

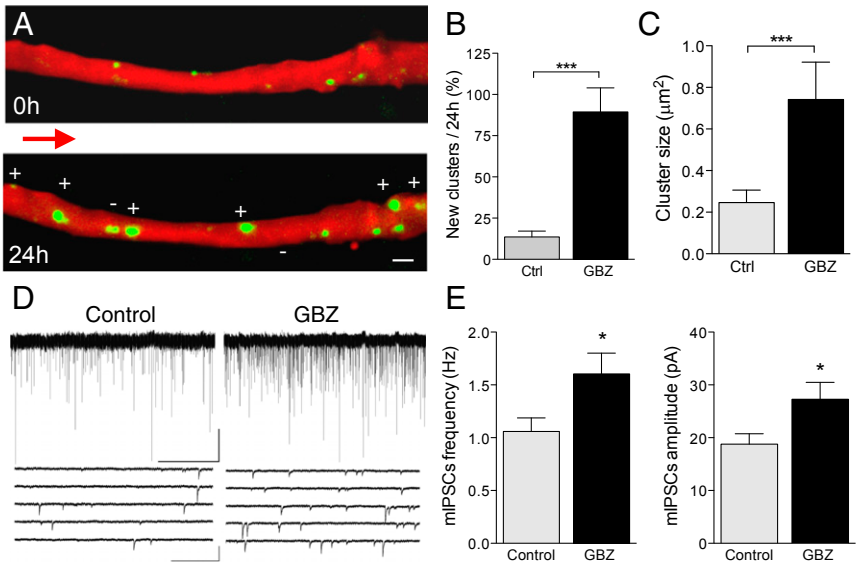

Fig. 3. Increase in gephyrin cluster dynamics by the $GABA_AR$ antagonist gabazine (GBZ). (*A*) Proximal apical dendrite before and 24 h after a short GBZ treatment (45 min). Note the marked increase in number (+) and size of gephyrin clusters. (*B*) Proportion of new gephyrin clusters observed 24 h after a short GBZ treatment (Ctrl, open columns, $n = 7$ cells/57 clusters; GBZ, filled columns, $n = 7$ cells/36 clusters). (*C*) Changes in mean size of gephyrin clusters. (*D*) Illustration of mIPSCs recorded in nontransfected CA1 pyramidal neurons under control conditions (*Left*) and 24 h after a short GBZ treatment. (*E*) Increase in mIPSC frequency (*Left*) and amplitude (*Right*) induced by GBZ (Ctrl, open columns, $n = 11$ cells; GBZ, filled columns, $n = 11$ cells). (Scale bars: *A*, 2 μm; *D, Top Right*, 50 pA/50 s; *D, Bottom Right*, 100 pA/0.5 s.)

individual neurons (Fig. 4*B*; see *Methods* for details). Analysis of transfected neurons before and 24 h after light stimulation revealed that neurons exposed to 470-nm light pulses (blue), but not neurons exposed to 625-nm light pulses (red), showed very robust structural changes. The proportion of newly formed gephyrin clusters (red light, $n = 4$ cells; blue light, $n = 6$ cells; Fig. 4 *C–F* and Table S1) and their size (Fig. 4*G* and Table S1) strongly increased 24 h after stimulation. Similar results were also obtained when light stimulation was applied in the presence of glutamate receptor antagonists or TTX (Fig. 4 *C–F* and Table S1). These experiments thus indicated that cell spiking and depolarization were sufficient to promote inhibitory synapse formation.

Role of Ca^{2+}/Calmodulin-Dependent Protein Kinase II and Gephyrin Phosphorylation in Gephyrin Cluster Plasticity. To investigate the underlying molecular mechanisms, we first examined a possible implication of multifunctional Ca^{2+}/calmodulin-dependent protein kinase II (CaMKII), recently shown to accumulate at inhibitory synapses following glutamate stimulation (19). Treatment of slice cultures with the CaMKII inhibitor KN-93 (10 μM) during TBS fully prevented the activity-dependent increase in gephyrin cluster formation and size (Fig. 5 *A* and *B*). We then looked for a possible target of CaMKII. Because gephyrin phosphorylation is implicated in $GABA_ARs$ clustering (8), we analyzed CaMKII phosphorylation sites on gephyrin. In silico analysis of rat gephyrin sequences (NP_074056.2) identified two residues, S303 and S305, that had a strong consensus for CaMKII phosphorylation and we therefore generated gephyrin double mutants for these two sites. Later in vitro kinase assay with bacterially expressed and purified gephyrin and active forms of CaMKII and PKA revealed that S305 site is a target of CaMKII, whereas S303 site is phosphorylated by PKA (Fig. S4). Treatment with GBZ (15 μM) resulted in an enhanced phosphorylation of S305 site, but not of S303, as revealed by phospho-specific antibodies (Fig. 5*C* and Fig. S4). Comparison of immunostaining for gephyrin and pS305-gephyrin further showed that GBZ markedly increased the ratio of phosphorylation and size of gephyrin clusters (Fig. 5*D*). We then tested the S303A/S305A (phospho-deficient, SSA) and S303D/S305D (phospho-mimetic, SSD) eGFP-gephyrin double mutants and single S305A and S305D mutants on inhibitory plasticity. Analysis of fluorescent gephyrin cluster turnover showed that the phospho-resistant mutants (SSA and S305A) did not significantly affect basal gephyrin cluster dynamics (Fig. 5 *E* and *F* and Table S1). In contrast, the phospho-mimetic mutants (SSD and S305D) significantly increased cluster formation under basal conditions (Fig. 5 *E* and *F* and Table S1). Next, we tested their effects on activity-dependent mechanisms following TBS. Transfection of pyramidal neurons with the phospho-resistant mutants (SSA+TBS and S305A+TBS) fully prevented activity-dependent formation of new gephyrin clusters (Fig. 5 *E* and *F* and Table S1), indicating that gephyrin phosphorylation on S305 is necessary for activity-dependent inhibitory synapse formation. Conversely, transfection with the phospho-mimetic mutants (SSD+TBS and S305D+TBS) increased gephyrin cluster formation under basal conditions (Fig. 5*E*), an effect that occluded further increases by TBS (Fig. 5*F* and Table S1). These results thus indicate that phosphorylation of gephyrin on S305 site is both sufficient and necessary to promote inhibitory synapse formation in response to neuronal activity. Note that expression of the phospho-resistant mutants (SSA+TBS and S305A+TBS) also prevented all changes in size of gephyrin clusters by stimulation (Fig. 5*H* and Table S1). Interestingly, the differential regulation of cluster size by activity remained preserved with the phospho-mimetic mutants (SSD+TBS and S305D+TBS), independently of the effects on dynamics (Fig. 5*H* and Table S1). This result suggests that the regulation of gephyrin cluster size by activity requires additional sites or mechanisms.

Discussion

Work over the last decade has provided strong evidence that behavioral experience and learning can promote rearrangements of excitatory synaptic networks (20). The present study now demonstrates that the same activity patterns and neuronal depolarization also promote rearrangements of perisomatic inhibitory synapses in the hippocampus. Our study was carried out in organotypic slice cultures, which may differ from the in vivo situation, but share strong developmental similarities in terms of intrinsic connectivity and plasticity mechanisms (21–23).

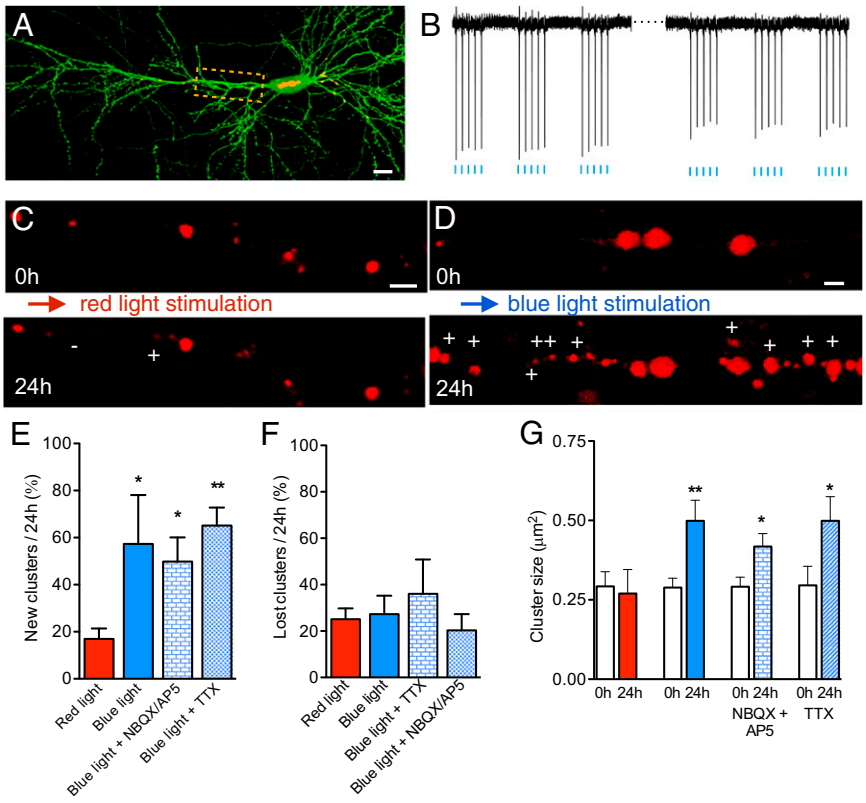

Fig. 4. Optogenetic activation of single pyramidal neurons increases gephyrin cluster dynamics. (*A*) CA1 pyramidal neuron expressing mCherry-gephyrin (red) and ChR2-venus (green). (*B*) Representative traces of cell attached recordings obtained at the beginning and end of a short (5 min, 1 Hz trains of five pulses at 10 Hz) optogenetic stimulation (470 nm blue light) of a cell expressing mCherry-gephyrin/ChR2-venus. Each vertical deflection represents an action potential. (*C*) Proximal apical dendrite showing new (+) and lost (-) mCherry-gephyrin clusters observed 24 h after a 5-min optogenetic stimulation with red light (625 nm). (*D*) Same as *C* but following 5-min stimulation with blue light (470 nm). Note the robust increase in new clusters. (*E*) Proportion of new gephyrin clusters observed following stimulation with red and blue light or blue light in the presence of DNQX (10 μM) and AP5 (50 μM) or TTX (1 μM; red light, red columns, $n = 4$ cells; blue light, blue columns, $n = 6$ cells; blue light + NBQX/AP5, $n = 3$ cells, blue light + TTX, $n = 3$ cells). (*F*) Same as *E* but for lost gephyrin clusters. (*G*) Changes in the mean size of gephyrin clusters under the same conditions. (Scale bars: *A*, 12 μm; *C* and *D*, 3 μm.)

Several forms of plasticity have been described at inhibitory synapses. Changes in strength of GABAergic transmission have been reported at many inhibitory synapses (3, 4, 24) and shown to involve different molecular events (25, 26). The notion that inhibitory synapses could also be structurally plastic and undergo continuous rearrangements is, however, much less understood. Recent in vivo studies have showed that sensory activity or ocular dominance plasticity are associated with important changes in the kinetics and clustering of dendritic inhibitory synapses (14, 15, 27). Here we focused on perisomatic inhibition, which is mainly mediated by parvalbumin interneurons and represents the main inhibitory input to hippocampal CA1 pyramidal neurons (28). These GABAergic synapses play an essential role in the control of network activity and gamma oscillations (29, 30). Using tagged gephyrin as a marker of inhibitory synapses, our study shows that patterns of high frequency activity and neuronal firing promote the formation of new gephyrin clusters within hours. This result is unlikely to be due to gephyrin overexpression, because overexpression of wild-type gephyrin did not affect spontaneous inhibitory transmission or cluster size or density (refs. 8 and 31; Fig. S2). Several findings suggest that the new gephyrin clusters induced by activity are new inhibitory synapses. Their size correspond to that revealed by endogenous gephyrin immunostaining and values obtained by nanoscopic analysis of gephyrin clusters (16). The new gephyrin clusters detected after stimulation display colocalization with GAD67 immunostaining and correlate with the presence of inhibitory symmetric synapses revealed by 3D EM reconstruction. A few inhibitory synapses were not detected at the confocal level by this approach (14, 15); however, they cannot account for the magnitude of changes reported here. Finally, whole cell recordings and immunolabeling of gephyrin clusters in nontransfected cells are also consistent with an increased number and efficacy of inhibitory synapses. Altogether, these results support the conclusion that synaptic and neuronal activity promoted the formation of new perisomatic inhibitory contacts.

Our experiments further identify one phosphorylation site on gephyrin that appears to be both necessary and sufficient for the formation of new inhibitory synapse by activity. The critical involvement of gephyrin in these mechanisms is consistent with several recent data highlighting its implication in the clustering of $GABA_A$Rs. Phosphorylation of gephyrin on Ser270 by glycogen synthase kinase 3β (GSK3β) or on Ser268 by ERK have been shown to modulate the density and size of gephyrin clusters (8, 31). Also gephyrin can interact with various partners, including neuroligin 2, collibystin, or even Cdc42 to regulate cluster formation and $GABA_A$R aggregation (7, 9). These results are thus consistent with the idea that gephyrin acts as a molecular hub regulating the formation and extension of the inhibitory postsynaptic density (12). Our data now indicate that gephyrin phosphorylation on Ser305 plays a critical role in the activity-dependent regulation of these clustering mechanisms. Our results further suggest that CaMKII is directly implicated in this effect. Pharmacological blockade of CaMKII prevented gephyrin cluster dynamics, S305 is phosphorylated by CaMKII, and its phosphorylation is enhanced following neuronal activation.

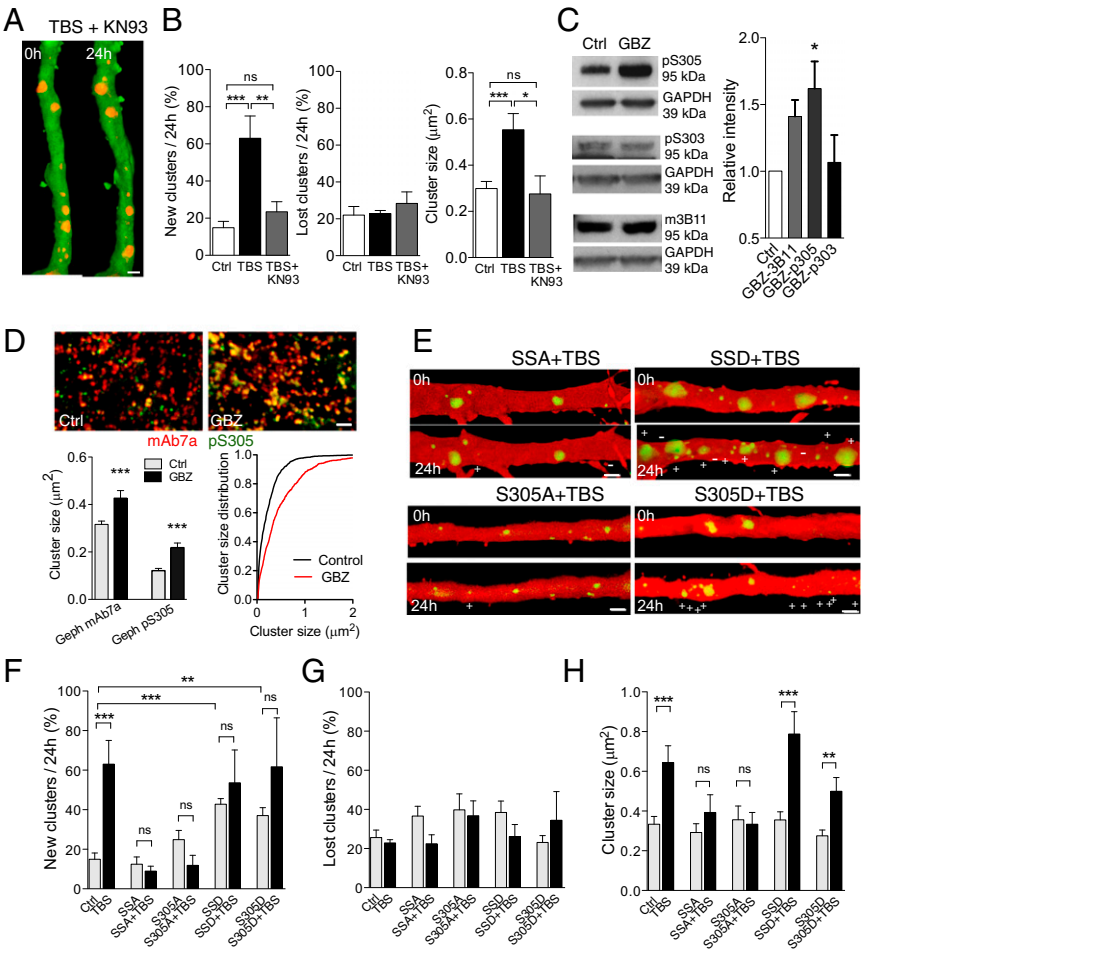

Fig. 5. Inhibitory synapse formation through CaMKII-mediated phosphorylation of gephyrin. (*A*) mCherry-gephyrin clusters (red) observed on a proximal apical dendrite (green) before and 24 h after TBS stimulation applied in the presence of KN-93 (10 μM). (*B*) TBS-induced gephyrin cluster dynamics is blocked by KN-93 (10 μM). (*C*) Increased phosphorylation of S305 but not S303 by GBZ treatment. (*D*) Endogenous gephyrin clusters observed before (Ctrl) and 24 h after GBZ treatment. Clusters are revealed by a double immunostaining using the mAb7a antibody against wild-type gephyrin (red) and the pS305 phospho-specific antibody (green). Note the marked increase in colocalization (yellow) observed after GBZ treatment, pointing to an increased phosphorylation of gephyrin on S305. *Left* shows the changes in mean cluster size revealed by the two antibodies, and in *Right*, the cluster size distribution under the two conditions. (*E*) Illustration of gephyrin cluster dynamics induced by TBS in neurons transfected with S303A/S305A (SSA), S305S, S303D/S305D (SSD), and S305D mutants. (*F*) New gephyrin clusters observed over 24 h in control conditions and after TBS in neurons transfected with WT gephyrin, S303A/S305A, S305A, S303D/S305D, and S305D mutants. (*G*) Same as *F* but for lost gephyrin clusters. (*H*) Changes in gephyrin cluster size under the same conditions. (Scale bars: 2 μm.)

Finally interference with S305 phosphorylation through mutation either prevented or mimicked activity-dependent inhibitory synapse formation. Thus, CaMKII, which plays a key role in mechanisms of excitatory synapse plasticity (32), also mediates a compensatory increase of inhibitory synapse formation. In this regard, our results are very consistent with recent data showing that CaMKII, via a phosphorylation of $GABA_AR$, contributes to an activity-induced potentiation of GABAergic transmission (4).

Our data identify a mechanism through which neuronal activity can exert a homeostatic control of the number and function of perisomatic inhibitory synapses. This phenomenon may be critically important to individually optimize the level of inhibition on pyramidal neurons and, thus, set the proper balance required for the synchronization of oscillations mediated by parvalbumin interneurons during learning (29, 33, 34).

Methods

Organotypic Hippocampal Cultures. Organotypic hippocampal slice cultures (400 μm thick) were prepared from 6- to 7-d old rat pups (35) using a protocol approved by the Geneva Veterinary Office and transfected at DIV11 by using a biolistic approach (DNA-coated gold microcarriers; 1.6 μm with a Helios Gene Gun; Bio-Rad Laboratories) according to the instructions of the manufacturer. A few cells were usually transfected per slice, and only one cell per slice was analyzed by using repetitive confocal microscopy 8 d after transfection. Carbachol (10 μM, 45 min) was used to trigger theta activity, and gabazine (15 μM, 45 min) to block $GABA_AR$ (36) and induce epileptiform activity.

Plasmids and Gephyrin Phosphorylation Mutants. To visualize inhibitory synapses, we used eGFP-gephyrin (31) and mCherry-gephyrin (8). The double gephyrin mutants of the S303 and S305 residues were identified as putative CaMKII phosphorylation sites by in silico analyses (NP_074056.2). The double mutant eGFP-S303/S305A and eGFP-S303D/S305D gephyrin as well as the single eGFP-S305A and eGFP-S305D were generated by using a site-directed mutagenesis protocol (Life Technologies). The mutation sequences were confirmed and checked for protein expression before neuron transfection.

Imaging. Laser scanning confocal microscopy was performed by using an Olympus Fluoview 300 system. Proximal dendrites of CA1 hippocampal pyramidal neurons expressing tagged gephyrin were imaged 8 d after transfection at DIV19 for several days as described (18). For quantitative analyses, maximum intensity projections were used and images of proximal dendrites were thresholded from background with a scaling factor of 3 (segmentation plugin, NIH ImageJ). Gephyrin clusters were identified (regions of interest;

ROI) by using a multiparticle analysis by size discrimination (>0.02 μm^2, NIH ImageJ), and ROI area values were obtained from the z stack of raw images by using Multi Measure tool. Large gephyrin clusters of more than 1.5 μm^2 were excluded from quantitative analyses. For presentation purposes, images were processed with NIH ImageJ and OsiriX software for volume rendering.

EM. For correlative confocal and electron microscopy, hippocampal slice cultures with CA1 pyramidal neurons cotransfected with eGFP and mCherry-gephyrin were imaged in a confocal microscope, fixed, and processed for eGFP immunoperoxidase EM labeling as described (37). After embedding in EPON resin (Fluka), the slices were trimmed around the imaged neurons and serial ultrathin (60 nm) sections were cut. Images of the labeled primary apical dendrites of interest were taken at magnification 9,700× (Tecnai G212; FEI Company). After alignment of digital serial electron micrographs by using Photoshop software (Adobe), complete 3D reconstruction of the dendritic segment of interest was carried out by using Neurolucida software (version 6.02; MicroBrightField). Inhibitory synaptic contacts were defined by the presence of the close apposition of a presynaptic bouton, filled with pleomorphic synaptic vesicles forming an active zone with docked vesicles, with the labeled apical dendrite.

Optogenetic Stimulation. Slice cultures were transfected with Channelrhodopsin2-venus (ChR2-venus) and mCherry-gephyrin by using the gene gun approach. Eight days after transfection, they were transferred to a recording chamber and optogenetic stimulation was carried out by using laser-emitting diodes (488 nm and 625 nm). A 625-nm red light spot of ~100 μm in diameter was used to position the focus of the light over the cell of interest. Optogenetic stimulation was performed by using light pulses of 20-ms duration with a nominal power at the exit of 0.790 and 0.653 mW for blue and red light, respectively. The stimulation protocol consisted in five pulses at 10 Hz repeated every second for 5 min (1,500 pulses). Analyses were restricted to cells expressing equivalent levels of ChR2-venus and mCherry-gephyrin.

Electrophysiology. Stimulation of slice cultures was carried out in an interface chamber as described (18). They were continuously perfused (2–2.5 mL/min) with a solution containing (in mM): NaCl 124, KCl 1.6, $CaCl_2$ 2.5, $MgCl_2$ 1.5, $NaHCO_3$ 24, KH_2PO_4 1.2, glucose 10, and ascorbic acid 2 and saturated with 95% O_2 and 5% CO_2 (pH 7.4; temperature 31 °C). Tetrodotoxin (TTX 1 μM) and SR95531 (Gabazine, 10–15 μM) were added to the perfusion solution for spontaneous inhibitory miniature recordings (mIPSC). Whole-cell recordings were carried out by using patch pipettes filled with a solution containing (in mM): 70 Kgluconate, 70 KCl, 2 NaCl, 2 $MgCl_2$, 10 Hepes, 1 EGTA, 2 MgATP, and 0.3 Na_2GTP at pH 7.3 corrected with KOH (290 mOsm). Under these recording conditions, activation of $GABA_A$ receptors resulted in inward currents at a holding potential (V_h) of –70 mV (E_{GABA} was approximately–15 mV). Recordings were obtained by using an Axopatch 200B (Molecular Devices), filtered at 2 kHz, and digitized at 5–10 kHz and stored on hard disk. Data acquisition and analysis were performed using pClamp 9. Custom written software (Detector; courtesy J. R. Huguenard, Stanford University, Stanford, CA) was used for analyzing miniature IPSCs events.

Immunohistochemistry. Slices were fixed by using 2% (vol/vol) cold paraformaldehyde in 0.1 M phosphate buffer for 1 h, rinsed with phosphate buffer saline (PBS), pH 7.4 for 45 min, and then simultaneously blocked and permeabilized for 1 h at room temperature in PBS containing 0.5–1% Triton X-100, 5–10% normal goat serum (NGS), and 1–2% BSA, pH 7.4. Slices were then incubated overnight at 4 °C in a tilting platform with either mouse monoclonal anti-GAD67 (1:5,000; MAB 5406, clone 1G10.2.; Millipore) or anti-gephyrin (1:500; 147021, clone mAb7; SYSY) antibodies dissolved in PBS containing 0.5% Triton X-100, 5% NGS, and 0.5% BSA, pH 7.4. After primary antibody incubation, slices were washed and incubated with Alexa Fluor 488 or 647 donkey anti-mouse (1:500; A21202, A11008; Invitrogen) secondary antibodies. The slices were mounted on slides in a 0.2% *n*-propyl gallate-based antifading solution. Sections were acquired with a confocal laser scanning microscope (LSM 510 Meta; Carl Zeiss) with 40× 0.8 W (3.6 mm) objective lens. Images were background subtracted and thresholded by using NIH ImageJ to include signals at least two- to threefold greater than the background signal.

Mouse Brain Extract and in Vitro Kinase Assay. Three-month-old mice whole brain extract was prepared through homogenization by using lysis buffer in the presence of protease inhibitor mixture (Roche) and phosphatase inhibitor 2 and 3 (Sigma). The total cell lysate was collected after ultracentrifugation of the samples at 76,862 × *g* for 60 min at 4 °C. Twelve milliliters of the sample was loaded on 8% SDS/PAGE gel and probed by using either phospho-gephyrin S303, phospho-gephyrin S305, and detected by using HRP-conjugated donkey secondary antibody (Jackson Laboratories).

In vitro kinase assay was performed by using purified full-length STREP-gephyrin expressed in bacteria (8). The purified gephyrin was phosphorylated in PKA kinase buffer (50 mM Mops pH 6.5, 100 μM ATP, 10 mM $MgCl_2$, 10 mM DTT, 1 mg/mL BSA, and H_2O to a final volume of 50 μL) or CaMKII kinase buffer (1× PK buffer, 1× $CaCl_2$, 1× CaM, and water to 50 mL) and 0.5 μL of purified activated PKA (Calbiochem) or 1 mL of CaMKII (NEB) was added and samples incubated at 30 °C for 30 min. The samples were washed in EBC buffer to remove all unbound kinase and proteins before addition of 2× SDS loading buffer and boiling at 90 °C for 3 min. Western blot to detect gephyrin phosphorylation was performed by using either anti–phospho-gephyrin Ser-303 (1 μg/mL, custom made by Genscript) or Ser-305 (1 mg/mL, custom made by Genscript) and Commassie stain to detect total gephyrin.

Western Blots. Slice cultures (16–20 DIV) were rapidly stored at −80 °C until homogenization. Tissue was lysed in lysis buffer (50 mM Tris pH 7.4–8, 120 mM NaCl, 0.5% Nonidet P-40) containing Complete miniprotease inhibitor (Roche Diagnostics) and phosphatase inhibitors (Sigma-Aldrich). Homogenates were sonicated at 4 °C, centrifuged for 20 min at 14,000 × *g* at 4 °C, and the supernatant was collected. Protein was quantified by using BCATM Protein Assay Kit (Pierce), and 20 μL of samples (containing 40 μg of protein) were resolved on Bis-Tris Protein Gels 4–12% (NuPAGE). To detect gephyrin phosphorylation, membranes were blocked for 1 h at room temperature with 5% nonfat dry milk in TBS and then probed by using either mouse monoclonal gephyrin antibody (1–1,000) (3B11, SYSY) or phospho-gephyrin S305 (1 mg/mL, custom made by Genscript), or rabbit polyclonal GAPDH antibody (1–50,000) (Sigma) antibodies and detected by using HRP-conjugated donkey secondary antibody (Jackson Laboratories). Proteins were resolved by chemiluminescence ECL (GE Healthcare).

Statistical Analyses. Graphs and statistical analyses were carried out with Prism. Data and statistics are given for each experimental condition in Table S1. Statistical analyses were performed by using unpaired *t* tests, unless otherwise indicated. Data are represented as mean ± SEM. Data significance is indicated as follows: $*P < 0.05$, $**P < 0.01$, $***P < 0.001$.

ACKNOWLEDGMENTS. We thank Yann Bernardinelli, Lorena Jourdain and all laboratory members for their support and excellent technical help. This work was supported by Swiss National Science Foundation Grant Sinergia and Grant 310030B-144080 (to D.M.).

1. Malinow R, Malenka RC (2002) AMPA receptor trafficking and synaptic plasticity. *Annu Rev Neurosci* 25:103–126.
2. Turrigiano GG, Nelson SB (2004) Homeostatic plasticity in the developing nervous system. *Nat Rev Neurosci* 5(2):97–107.
3. Nugent FS, Penick EC, Kauer JA (2007) Opioids block long-term potentiation of inhibitory synapses. *Nature* 446(7139):1086–1090.
4. Petrini EM, et al. (2014) Synaptic recruitment of gephyrin regulates surface GABAA receptor dynamics for the expression of inhibitory LTP. *Nat Commun* 5:3921.
5. Jacob TC, Moss SJ, Jurd R (2008) GABA(A) receptor trafficking and its role in the dynamic modulation of neuronal inhibition. *Nat Rev Neurosci* 9(5):331–343.
6. Fritschy JM, Panzanelli P, Tyagarajan SK (2012) Molecular and functional heterogeneity of GABAergic synapses. *Cell Mol Life Sci* 69(15):2485–2499.
7. Poulopoulos A, et al. (2009) Neuroligin 2 drives postsynaptic assembly at perisomatic inhibitory synapses through gephyrin and collybistin. *Neuron* 63(5):628–642.
8. Tyagarajan SK, et al. (2011) Regulation of GABAergic synapse formation and plasticity by GSK3beta-dependent phosphorylation of gephyrin. *Proc Natl Acad Sci USA* 108(1):379–384.
9. Tyagarajan SK, Ghosh H, Harvey K, Fritschy JM (2011) Collybistin splice variants differentially interact with gephyrin and Cdc42 to regulate gephyrin clustering at GABAergic synapses. *J Cell Sci* 124(Pt 16):2786–2796.
10. Mayer S, et al. (2013) Collybistin activation by GTP-TC10 enhances postsynaptic gephyrin clustering and hippocampal GABAergic neurotransmission. *Proc Natl Acad Sci USA* 110(51):20795–20800.
11. Vlachos A, Reddy-Alla S, Papadopoulos T, Deller T, Betz H (2013) Homeostatic regulation of gephyrin scaffolds and synaptic strength at mature hippocampal GABAergic postsynapses. *Cereb Cortex* 23(11):2700–2711.
12. Tyagarajan SK, Fritschy JM (2014) Gephyrin: A master regulator of neuronal function? *Nat Rev Neurosci* 15(3):141–156.

13. Dobie FA, Craig AM (2011) Inhibitory synapse dynamics: Coordinated presynaptic and postsynaptic mobility and the major contribution of recycled vesicles to new synapse formation. *J Neurosci* 31(29):10481–10493.
14. Chen JL, et al. (2012) Clustered dynamics of inhibitory synapses and dendritic spines in the adult neocortex. *Neuron* 74(2):361–373.
15. van Versendaal D, et al. (2012) Elimination of inhibitory synapses is a major component of adult ocular dominance plasticity. *Neuron* 74(2):374–383.
16. Specht CG, et al. (2013) Quantitative nanoscopy of inhibitory synapses: Counting gephyrin molecules and receptor binding sites. *Neuron* 79(2):308–321.
17. Lushnikova I, Skibo G, Muller D, Nikonenko I (2011) Excitatory synaptic activity is associated with a rapid structural plasticity of inhibitory synapses on hippocampal CA1 pyramidal cells. *Neuropharmacology* 60(5):757–764.
18. De Roo M, Klauser P, Muller D (2008) LTP promotes a selective long-term stabilization and clustering of dendritic spines. *PLoS Biol* 6(9):e219.
19. Marsden KC, Shemesh A, Bayer KU, Carroll RC (2010) Selective translocation of Ca2+/calmodulin protein kinase IIalpha (CaMKIIalpha) to inhibitory synapses. *Proc Natl Acad Sci USA* 107(47):20559–20564.
20. Caroni P, Donato F, Muller D (2012) Structural plasticity upon learning: Regulation and functions. *Nat Rev Neurosci* 13(7):478–490.
21. Gähwiler BH, Capogna M, Debanne D, McKinney RA, Thompson SM (1997) Organotypic slice cultures: A technique has come of age. *Trends Neurosci* 20(10):471–477.
22. Mellentin C, Møller M, Jahnsen H (2006) Properties of long-term synaptic plasticity and metaplasticity in organotypic slice cultures of rat hippocampus. *Exp Brain Res* 170(4):522–531.
23. Kehoe LA, et al. (2014) GluN3A promotes dendritic spine pruning and destabilization during postnatal development. *J Neurosci* 34(28):9213–9221.
24. Kullmann DM, Moreau AW, Bakiri Y, Nicholson E (2012) Plasticity of inhibition. *Neuron* 75(6):951–962.
25. Kano M, Ohno-Shosaku T, Hashimotodani Y, Uchigashima M, Watanabe M (2009) Endocannabinoid-mediated control of synaptic transmission. *Physiol Rev* 89(1): 309–380.
26. Vithlani M, Terunuma M, Moss SJ (2011) The dynamic modulation of GABA(A) receptor trafficking and its role in regulating the plasticity of inhibitory synapses. *Physiol Rev* 91(3):1009–1022.
27. Knott GW, Quairiaux C, Genoud C, Welker E (2002) Formation of dendritic spines with GABAergic synapses induced by whisker stimulation in adult mice. *Neuron* 34(2): 265–273.
28. Megías M, Emri Z, Freund TF, Gulyás AI (2001) Total number and distribution of inhibitory and excitatory synapses on hippocampal CA1 pyramidal cells. *Neuroscience* 102(3):527–540.
29. Bartos M, Vida I, Jonas P (2007) Synaptic mechanisms of synchronized gamma oscillations in inhibitory interneuron networks. *Nat Rev Neurosci* 8(1):45–56.
30. Kullmann DM (2011) Interneuron networks in the hippocampus. *Curr Opin Neurobiol* 21(5):709–716.
31. Tyagarajan SK, et al. (2013) Extracellular signal-regulated kinase and glycogen synthase kinase 3β regulate gephyrin postsynaptic aggregation and GABAergic synaptic function in a calpain-dependent mechanism. *J Biol Chem* 288(14):9634–9647.
32. Lisman J, Yasuda R, Raghavachari S (2012) Mechanisms of CaMKII action in long-term potentiation. *Nat Rev Neurosci* 13(3):169–182.
33. Sohal VS, Zhang F, Yizhar O, Deisseroth K (2009) Parvalbumin neurons and gamma rhythms enhance cortical circuit performance. *Nature* 459(7247):698–702.
34. Donato F, Rompani SB, Caroni P (2013) Parvalbumin-expressing basket-cell network plasticity induced by experience regulates adult learning. *Nature* 504(7479): 272–276.
35. Stoppini L, Buchs PA, Muller D (1991) A simple method for organotypic cultures of nervous tissue. *J Neurosci Methods* 37(2):173–182.
36. Jones MV, Jonas P, Sahara Y, Westbrook GL (2001) Microscopic kinetics and energetics distinguish GABA(A) receptor agonists from antagonists. *Biophys J* 81(5):2660–2670.
37. Nikonenko I, et al. (2008) PSD-95 promotes synaptogenesis and multiinnervated spine formation through nitric oxide signaling. *J Cell Biol* 183(6):1115–1127.